Journal of Biomolecular NMR, 8 (1996) 171–183
ESCOM



J-Bio NMR 360

# $^{1}H$, $^{13}C$ and $^{15}N$ NMR assignments and secondary structure of the paramagnetic form of rat cytochrome $b_5$

Siddhartha Sarma[a], Russell J. DiGate[a], Debra L. Banville[b] and R.D. Guiles[a,*]

[a]*Department of Pharmaceutical Sciences, University of Maryland at Baltimore, 20 North Pine Street and the Medical Biotechnology Center, University of Maryland Biotechnology Institute, 618 W. Lombard Street, Baltimore, MD 21201, U.S.A.*
[b]*Physical Sciences Department, Zeneca Pharmaceuticals, 1800 Concord Pike, P.O. Box 15437, Wilmington, DE 19850-5437, U.S.A.*

Received 9 February 1996
Accepted 8 April 1996

*Keywords:* 3D NMR; Paramagnetic; Heterogeneity; Cytochrome $b_5$

## Summary

Modern multidimensional double- and triple-resonance NMR methods have been applied to assign the backbone and side-chain $^{13}C$ resonances for both equilibrium conformers of the paramagnetic form of rat liver microsomal cytochrome $b_5$. The assignment of backbone $^{13}C$ resonances was used to confirm previous $^{1}H$ and $^{15}N$ resonance assignments [Guiles, R.D. et al. (1993) *Biochemistry*, **32**, 8329–8340]. On the basis of short- and medium-range NOEs and backbone $^{13}C$ chemical shifts, the solution secondary structure of rat cytochrome $b_5$ has been determined. The striking similarity of backbone $^{13}C$ resonances for both equilibrium forms strongly suggests that the secondary structures of the two isomers are virtually identical. It has been found that the $^{13}C$ chemical shifts of both backbone and side-chain atoms are relatively insensitive to paramagnetic effects. The reliability of such methods in anisotropic paramagnetic systems, where large pseudocontact shifts can be observed, is evaluated through calculations of the magnitude of such shifts.

## Introduction

Cytochrome $b_5$ is a small heme-containing redox protein that is present in a membrane-bound form in the smooth endoplasmic reticulum of liver microsomal cells and in a water-soluble form in erythrocytes. The primary sequence is highly conserved among various mammalian and avian species (for a review, see Mathews, 1985). This heme protein is unusual in its functional diversity, in that it participates in a variety of electron-transfer reactions. In the liver it is involved in the NADH-linked desaturation of fatty acids (Ohsino and Sato, 1971; Shimakata et al., 1972; Strittmatter et al., 1974). Cytochrome $b_5$ also supplies electrons to cytochrome P450 in a number of hydroxylation reactions (Cohen and Estabrook, 1971; Hildebrandt and Estabrook, 1971; Imai and Sato, 1977). In the erythrocytes its function is to reduce methemoglobin and thus maintains the physiological status of hemoglobin as an oxygen carrier (Hultquist et al., 1984).

The crystal structure of lipase-solubilized calf-liver cytochrome $b_5$ has been determined by X-ray diffraction to a resolution of 2 Å (Mathews et al., 1979). Nuclear

*To whom correspondence should be addressed.

*Abbreviations:* DANTE, delays alternating with nutation for tailored excitation; DEAE, diethylaminoethyl; DQF-COSY, 2D double-quantum-filtered correlation spectroscopy; EDTA, ethylenediaminetetraacetic acid; HCCH-TOCSY, 3D proton-correlated carbon TOCSY experiment; HMQC, 2D heteronuclear multiple-quantum correlation spectroscopy; HNCA, 3D triple-resonance experiment correlating amide protons, amide nitrogens and alpha carbons; HNCO, 3D triple-resonance experiment correlating amide protons, amide nitrogens and carbonyl carbons; HNCOCA, 3D triple-resonance experiment correlating amide protons, amide nitrogens and alpha carbons via carbonyl carbons; HOHAHA, 2D homonuclear Hartmann–Hahn spectroscopy; HOHAHA-HMQC, 3D HOHAHA relayed HMQC; HSQC, 2D heteronuclear single-quantum correlation spectroscopy; IPTG, isopropyl thiogalactoside; NOESY, 2D nuclear Overhauser enhancement spectroscopy; NOESY-HSQC, 3D NOESY relayed HSQC; TOCSY, 2D total correlation spectroscopy; TPPI, time-proportional phase incrementation; TSP, trimethyl silyl propionate.

*Supplementary Material:* three figures, illustrating the sequential connectivity path in the 3D HNCA (Fig. S-1), a 3D $^{15}N$-edited NOESY-HSQC (Fig. S-2) for the entire protein and side-chain assignments from the HCCH-TOCSY spectrum for some of the residues (Fig. S-3). One table (Table S-1), containing nearly complete $^{1}H$, $^{13}C$ and $^{15}N$ assignments for rat-liver microsomal ferricytochrome $b_5$ is also available.

magnetic resonance studies have shown that cytochrome $b_5$ exists in solution as a mixture of two conformers (Keller et al., 1976). The origins of this heterogeneity are well understood; it is caused by a rotation of the heme cofactor by 180° about the α,γ-meso-axis within the heme binding pocket (La Mar et al., 1981). Additionally, the relative abundance of the two conformers is species-dependent (McLachlan et al., 1986).

Given the wealth of structural information available, and due to the variety of systems that it interacts with, cytochrome $b_5$ has become a model protein to study by experimental and theoretical methods. For example, the molecular mechanisms of interprotein electron transfer (Salemme, 1976; Wendoloski et al., 1987), the specificity of protein–protein interactions (Sligar et al., 1987; Rodgers et al., 1988) and the mechanisms by which proteins control heme redox potentials (Funk et al., 1990) have been studied in some detail.

Our interest lies in determining protein factors that control heme reduction potentials and the specificity of protein–protein interactions during the electron-transfer process using rat cytochrome $b_5$ as a model. Although many species variants of cytochrome $b_5$ have been isolated and characterized, the rat cytochrome $b_5$ is unique in that it has the maximal detectable heterogeneity in solution (ratios of major and minor forms range from chicken 20 : 1, calf 8.9 : 1 to 6 : 4 for the rat; Lee et al., 1994). The reason for the shift in conformer distribution has been attributed to the relative steric bulk of the residues at positions 23 and 25 in the amino acid sequence. The chicken protein contains an isoleucine amino acid at position 23, whereas the bovine and rat proteins contain a leucine and a valine residue, respectively. The chicken protein differs from the bovine and rat proteins at position 25 in that it contains a valine instead of a leucine residue. Irrespective of the distribution ratio, the two forms differ in reduction potential by 27 mV (Walker et al., 1988).

Our goal is to determine the high-resolution solution structure of both conformers of rat cytochrome $b_5$ using modern multinuclear, multidimensional NMR methods. NMR methods are most suitable for this system because of its small size and high solubility. Other high-resolution structural methods, such as X-ray crystallography, are nearly intractable for this particular species variant because of the static disorder introduced by the conformers. The rat cytochrome $b_5$ is the most heterogeneous system that has been assigned using 2D homo- and heteronuclear NMR methods (Guiles et al., 1992,1993). However, given the complexity of the assignment problem (an almost 40% increase in resonances because of the two conformers), there is always potential for overlap resulting in ambiguity of resonance assignments. This problem is further exacerbated when attempting to assign the paramagnetic form of the protein, given the increased line widths and missing correlation peaks, due to efficient dipolar relaxation induced by the paramagnetic center.

This study extends the previous $^1H$ and $^{15}N$ assignments to include $^{13}C$ resonance assignments of rat ferricytochrome $b_5$. We have applied 3D triple-resonance heteronuclear multidimensional NMR experiments (Bax and Grzesiek, 1993) to obtain sequential connectivities based on scalar coupling between backbone $^{13}C$ and $^{15}N$ nuclei. Sequential NOE correlations obtained from 3D double-resonance experiments were used as an independent connectivity path to confirm triple-resonance assignments and to sort out overlapping correlation peaks. Carbon-13 resonances of $C^\alpha$ and CO nuclei were compared to random-coil values for secondary shifts in order to qualitatively analyze the secondary structure of rat ferricytochrome $b_5$. The secondary structure analysis relied on NOE correlations observed in 2D and 3D spectra. The reliability of such methods in anisotropic paramagnetic systems, where large pseudocontact shifts can be observed, is evaluated through calculations of the magnitude of such shifts.

## Materials and Methods

*Plasmid construction*

The synthetic gene coding for the soluble heme binding domain of the rat cytochrome $b_5$ in a pUC13 plasmid (Von Bodman et al., 1986) was subcloned into an overexpression vector pET3C, an IPTG-inducible vector containing a T7 RNA polymerase promoter and a high-affinity ribosome binding site. Detailed properties of this expression vector have been described elsewhere (Studier et al., 1990).

Reengineering of the plasmid was accomplished in the following manner. A unique NdeI restriction site was introduced at the initiation codon of the gene using PCR-mediated amplification (Saiki et al., 1988). The amplified gene could then be ligated into the pET3C vector using NdeI and EcoRI restriction sites. *E. coli* strain BL-21 (PlysS) (which has the T7 RNA polymerase gene in its chromosome under the control of a lac UV5 promoter) was transformed with the pET3C vector containing the rat cytochrome $b_5$ gene. T7 RNA polymerase could then be expressed by the addition of IPTG to the media, resulting in the dramatic overexpression of cytochrome $b_5$.

*Purification and labeling of rat cytochrome $b_5$*

Unlabelled cytochrome $b_5$ was produced by growing cells at 37 °C in rich medium. Induction of protein expression was achieved by the addition of 0.5 mM IPTG when the cells had grown to an OD of 0.6–0.8 at 590 nm. Cells were harvested 4 h after induction and disrupted by treatment with lysozyme. Reconstitution of the apoprotein was accomplished using the procedure described by Walker et al. (1988). Estimates of rat cytochrome $b_5$ in

the lysates were made by measuring the absorbance at 413 nm using a millimolar absorptivity of 117 (Strittmatter and Velick, 1956).

Purification of rat cytochrome $b_5$ involves several modifications of the published procedure (Von Bodman et al., 1986). The reconstituted crude extract was loaded onto a DEAE-Sephacel (Pharmacia, Piscataway, NJ, U.S.A.) column that was previously equilibrated with 50 mM Tris-HCl, pH 8.0, at 22 °C, 1 mM EDTA (Buffer A). The column was washed with two column volumes of buffer and the protein was eluted with a 0–0.4 M KCl salt gradient (in Buffer A). Fractions containing cytochrome $b_5$ at concentrations greater than 20% of the maximum were pooled together, Amicon-concentrated and loaded on a G-100 Sephadex (Pharmacia) column and eluted with Buffer A. Fractions with A413/A280 absorbance ratios greater than 4.5 were pooled together after cross-checking with gel electrophoresis and loaded onto a hydroxyl apatite column (Biorad, Hercules, CA, U.S.A.) and eluted with a 0–0.5 M $(NH_4)_2SO_4$ gradient in Buffer A (prepared without EDTA). Fractions with an A413/A280 ratio > 5.85, and which showed a single band on gel electrophoresis, were pooled together and dialysed against 100 mM $NH_4HCO_3$, lyophilized, and used in the biophysical studies described below. The above procedure yielded 90–100 mg of pure protein per liter of culture (rich medium).

Similar yields were obtained when the protein was expressed in M9 minimal media (McIntosh et al., 1987). Uniformly $^{15}N$-enriched wild-type protein was prepared by growing cells in M9 minimal media in which $^{15}NH_4Cl$ (Cambridge Isotopes, Woburn, MA, U.S.A.; 99% $^{15}N$) was used as the sole source of nitrogen. Uniformly $^{13}C$- and $^{15}N$-enriched double-labelled sample was prepared by adding $^{13}C$-labelled glucose (Isotec Inc., Miamisburg, OH, U.S.A.; 99% $^{13}C$) and $^{15}NH_4Cl$ as the sole sources of carbon and nitrogen. Due to the high cost of $^{13}C$-labelled glucose, it was added to a final concentration of 2 g/l of M9 medium. The yields however, dropped to 40 mg of pure protein per liter. Protein fractions that had a A413/A280 ratio > 5.9 and that showed a single band on SDS-PAGE gel electrophoresis were pooled, concentrated and lyophilized.

*NMR sample preparation*

NMR samples were prepared by dissolving purified rat cytochrome $b_5$ in 100 mM phosphate buffer, pH 7.2, prepared in 90% $H_2O$ (10% $D_2O$). The pH of the solution was adjusted to 7.00 by addition of small aliquots of 0.1 M NaOH. TSP was added to a final concentration of 1 mM as an internal chemical shift standard and the volume adjusted to 0.5 ml. Samples containing 100% $D_2O$ were prepared in a similar manner and subsequently lyophilized and exchanged with $D_2O$ (Cambridge Isotopes, 99.996% D) repeatedly. The dissolution step employed 99.996% $D_2O$. The NMR tube was then sealed under vacuum with a gas-oxygen torch. The pH values reported are uncorrected for deuterium isotope effects. Nitrogen-15-edited NMR data were acquired using a 8-mM sample of ferricytochrome $b_5$. Triple resonance and $^{13}C$-edited NMR data were acquired using a 5-mM sample of ferricytochrome $b_5$. Concentrations of the ferric protein were determined using an absorption coefficient of 117 $mM^{-1}$ at 413 nm (Strittmatter and Velick, 1956).

*NMR data acquisition*

All NMR spectra were recorded at 40 °C. The 3D HCCH-TOCSY experiment was acquired using a sample dissolved in $D_2O$. All other spectra were recorded using samples dissolved in $H_2O$. 2D $^1H$ homonuclear NMR spectra (DQF-COSY, HOHAHA and NOESY) are those reported earlier (Guiles et al., 1993). 2D $^1H$-$^{15}N$ HSQC (Bodenhausen and Ruben, 1980) and 3D $^{15}N$-edited NOESY-HSQC spectra (Kay et al., 1989; Marion et al., 1989a) were recorded on an OMEGA-PSG 600 NMR (599.71 MHz, $^1H$) spectrometer. For $^1H$-$^{15}N$ correlation, spectrum saturation of the $H_2O$ resonance was achieved using the DANTE water-suppression sequence (Zuiderweg et al., 1986). For the $^{15}N$-edited 3D NOESY-HSQC experiment water suppression was achieved using phase-ramped SLR-shaped pulses (Shinnar et al., 1989).

3D $^{15}N$-edited 'clean' HOHAHA-HMQC (Marion et al., 1989b), HNCOCA (Bax and Ikura, 1991), HNCO (Kay et al., 1990), and HCCH-TOCSY (Bax et al., 1990) spectra were recorded on a Bruker AMX 500 (500.13 MHz, $^1H$) spectrometer equipped with a triple-resonance probe. Solvent suppression in the HOHAHA-HMQC, HNCOCA and HNCO experiments was achieved using on-resonance presaturation during the relaxation delay. In the HCCH-TOCSY experiment, an off-resonance phase-ramped DANTE pulse was used to suppress the residual solvent signal. 3D HNCA (Grzesiek and Bax, 1992) spectrum was acquired on a Bruker DMX-600 (600.13 MHz, $^1H$) spectrometer equipped with a triple-resonance gradient probe. Pulsed field gradients were applied along the z-axis to purge undesired transverse magnetization (Bax and Pochapsky, 1992).

2D $^1H$-$^{15}N$ correlation spectra were recorded with proton and nitrogen spectral widths of 6006.01 and 2500 Hz, respectively. The spectrum was recorded with 512 $t_1$ increments to give a final matrix of 1024* $t_2 \times 512$* $t_1$ points. Phase-sensitive detection in the $t_1$ dimension was achieved by the method of States et al. (1982).

3D $^{15}N$-edited NOESY-HSQC spectra were recorded using a NOE mixing time of 150 ms, with spectral widths of 4608.29 Hz in F1 ($^1H$), 7142.86 Hz in F2 ($^1H$) and 2500 Hz in F3 ($^{15}N$). The size of the acquired matrix was

* denotes complex data points.

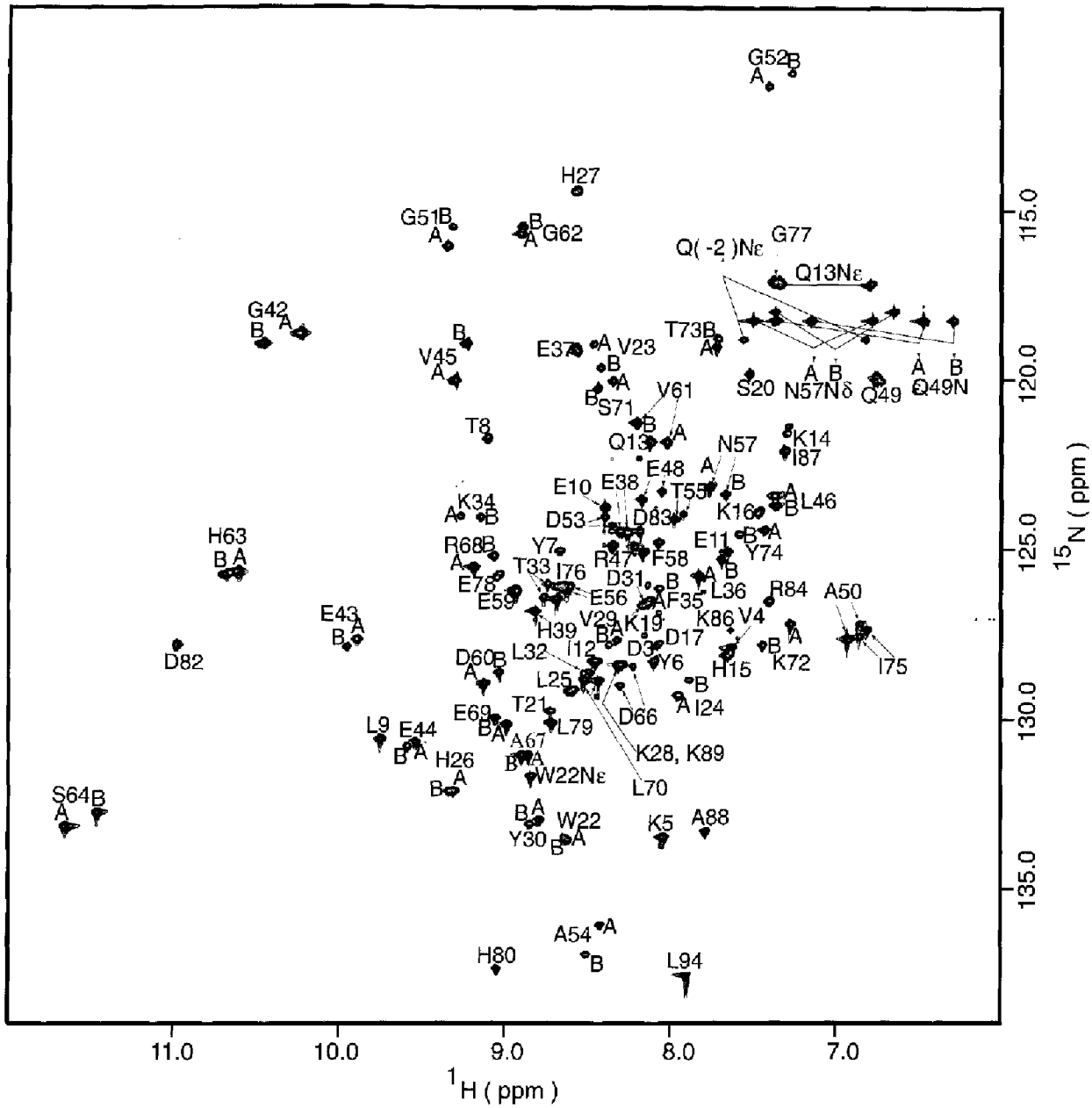


Fig. 1. 2D $^{1}H$-$^{15}N$ HSQC spectrum of uniformly $^{15}N$-labelled rat ferricytochrome $b_5$ recorded at 600-MHz proton frequency. Correlation peaks are labelled according to the residue type and sequence number. Isomer-specific assignments are shown as A and B (major and minor) forms for a majority of the residues, except for those centered between 8 and 8.5 ppm in the proton dimension, and between 125 and 128 ppm in the nitrogen dimension, due to spectral crowding. Isomer-specific assignments for side-chain amide atoms are indicated with connecting lines. The spectrum was recorded at 40 °C. Sample conditions are as described in the text.

$512 \times 256^* \times 64^*$. Quadrature detection in $t_1$ and $t_2$ was accomplished using the method of States et al. (1982).

3D $^{15}N$-edited HOHAHA-HMQC spectra were recorded using a 70-ms spin-lock (mixing time) period. Spectral widths of 4504.54 Hz in F1 ($^{1}H$), 13 200 Hz in F2 ($^{1}H$) and 1775 Hz in F3 ($^{15}N$) were used. The size of the acquired matrix was $512^* \times 256 \times 64$. Quadrature detection in $t_1$ and $t_2$ was accomplished using TPPI (Marion and Wüthrich, 1983).

3D HNCOCA and HNCO spectra were recorded with spectral widths of 9259.26 Hz in F1 ($^{1}H$), 1770 Hz in F2 ($^{15}N$) in both cases, and with 5030.35 Hz in F3 ($^{13}C$) for the HNCOCA experiment and 3270.32 Hz in F3 ($^{13}C$) for the HNCO experiment, respectively. The size of the acquired matrix for both experiments was $1024^* \times 80 \times 100$ data points. Quadrature detection in $t_1$ and $t_2$ was accomplished using TPPI (Marion and Wüthrich, 1983). The 3D HNCA spectra were recorded with spectral widths of 9803.92 Hz in F1 ($^{1}H$), 7507.51 Hz in F2 ($^{13}C$) and 2502.5 Hz in F3 ($^{15}N$). The size of the acquired matrix

was 1024×128*×64*. Complex data in $t_1$ and $t_2$ dimensions were acquired in a States-TPPI manner (Marion et al., 1989c). The HCCH-TOCSY experiment was acquired with spectral widths of 5000 Hz in F1 ($^1$H), 5000 Hz in F2 ($^1$H) and 3448.48 Hz in F3 ($^{13}$C).

*Data processing*

All data were transferred onto Silicon Graphics workstations and processed using FELIX v. 2.3 NMR processing software (Biosym Technologies Inc., San Diego, CA, U.S.A.). Time domain data of the indirectly detected dimensions were increased 25% by linear prediction (Olejniczak and Eaton, 1990). The resulting data were multiplied by a 80°-squared sinebell and zero-filled; final 3D matrices consisted of 512×512×256, 512×512×128, 512×256×128, 512×256×128, 512×256×128 and 512×512×256 real points for NOESY-HSQC, HOHAHA-HMQC, HNCA, HNCOCA, HNCO and HCCH-TOCSY experiments, respectively.

## Results

*Sequential assignment of rat cytochrome $b_5$*

The assignment strategy we employed relied upon 3D triple-resonance through-bond correlation experiments, as described by Kay et al. (1990). Firstly, we assigned backbone $^{15}$N, $^1$H and $^{13}$C resonances employing HNCA, HNCOCA and HNCO experiments. These assignments

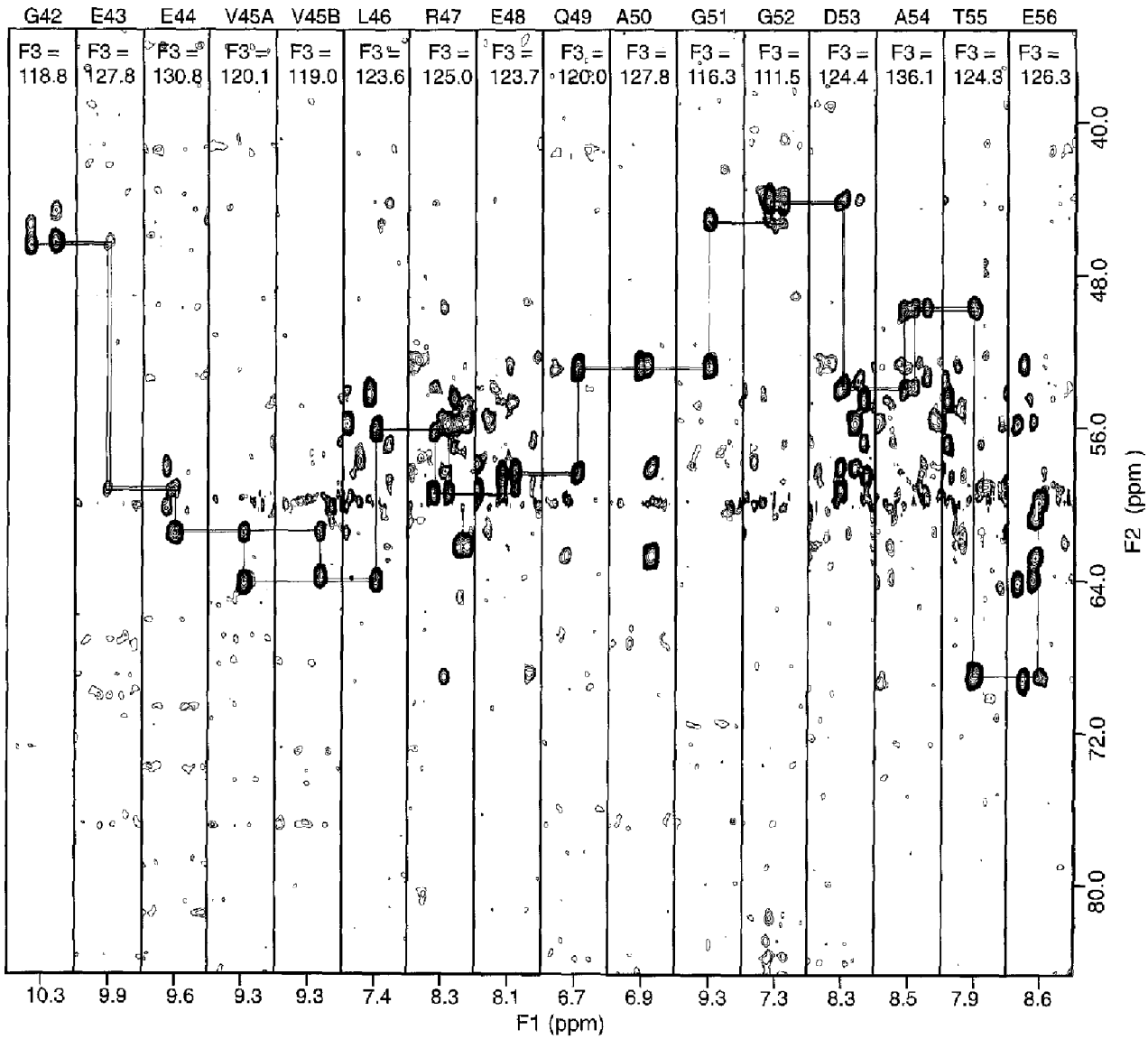


Fig. 2. 2D sections of the HNCA 3D experiment, indicating sequential connectivities for Gly$^{42}$ through Glu$^{56}$. Each residue is presented as a small region of the 2D spectrum taken at the $^{15}$N frequency and centered at the H$^N$ frequency (Table I). The $^{15}$N frequency of the more abundant isomer corresponding to the shown plane is indicated at the top of each panel. Unambiguous assignments of both equilibrium forms can be traced in the HNCA spectrum. In this region of the protein, consisting of two bends and one helix (Helix III, Glu$^{43}$–Ala$^{50}$), there is overlap between only one C$^\alpha$(i)-C$^\alpha$(i+1) pair, i.e. Glu$^{49}$ and Ala$^{50}$. F1 = $^1$H (ppm); F2 = $^{13}$C (ppm); and F3 = $^{15}$N (ppm).

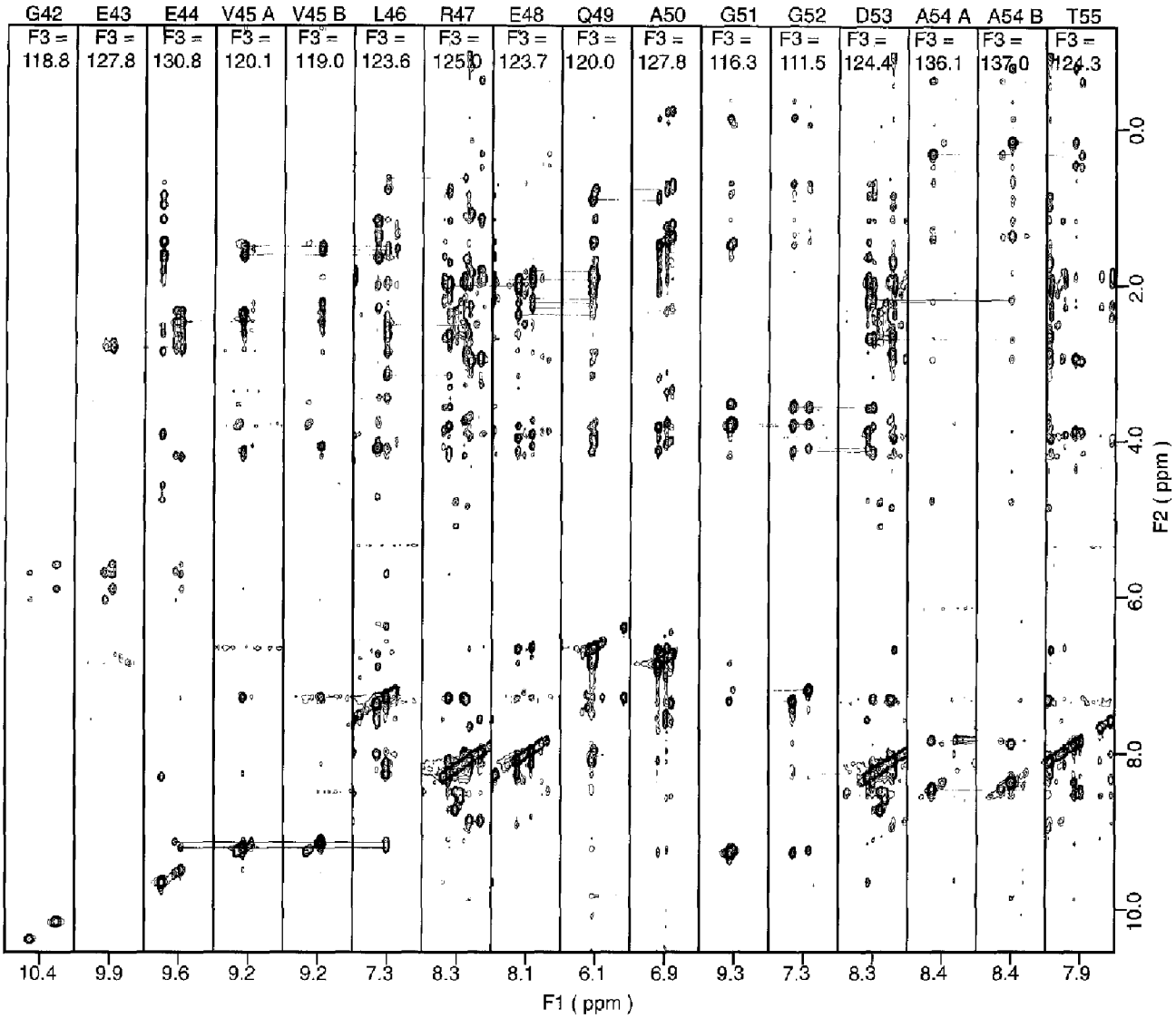


Fig. 3. 2D representation of the 3D $^{15}$N-edited NOESY-HSQC spectrum showing the sequential assignments for the same region of the protein as in Fig. 2. While clearly resolved peaks for both isomer forms are not observed for all residues, e.g. Glu$^{43}$, Gly$^{44}$, Gln$^{49}$, Asp$^{53}$ and Thr$^{55}$ in the HNCA spectrum (Fig. 2), the A and B isomers are clearly distinguishable in the NOESY-HSQC spectrum. F1 = $^{1}$H (ppm); F2 = $^{1}$H (ppm); and F3 = $^{15}$N (ppm).

were independently confirmed and ambiguities due to overlap were resolved through complete sequential assignments obtained from analysis of 3D NOESY-HSQC and HOHAHA-HMQC experiments. Side-chain assignments were then completed based on the analysis of HCCH-TOCSY and $^{13}$C-$^{1}$H HSQC spectra. Sequential assignments could also be confirmed, in part, through amino-acid-type identification through an analysis of $C^{\alpha}$ and $C^{\beta}$ chemical shifts (Grzesiek and Bax, 1993). Table S-I (Supplementary Material) contains a complete listing of the assignments obtained.

Figure 1 shows a 600 MHz $^{1}$H-$^{15}$N HSQC spectrum of rat ferricytochrome $b_5$, labelled with corresponding amino acid residues and sequence numbers for both equilibrium forms of the protein (the major abundance isomer is designated as 'A' and the minor as 'B'). The spectrum also shows assignments for 12 correlation peaks arising from side-chain amide groups of one asparagine and three glutamine residues. Two pairs for the major and minor forms of Asn$^{57}$, two pairs for Gln$^{49}$, one for Gln$^{13}$. Although we have been unable to assign the backbone atoms of Gln$^{-2}$ (see Mathews et al. (1979) for sequence numbering), the remaining pair by exclusion must belong to Gln$^{-2}$, since it is the only other residue in the sequence with a side-chain amide group.

Extensive $^{1}$H and $^{15}$N resonance assignments available from previous 500 MHz studies (Guiles et al., 1993), served as starting points in the sequential assignment process using the 3D HNCA and HNCOCA triple-resonance data. In total, resolved $C^{\alpha}$, $C^{\alpha}$(i–1) correlations were observed in the HNCA spectrum, for both equilibrium binding forms, for 73 out of 95 possible amino acids (98

TABLE I
$^1$H AND $^{15}$N CHEMICAL SHIFTS OF REASSIGNED RESIDUES OF RAT FERRICYTOCHROME $b_5$

| Residue | Form | Previous δ (ppm)[a] | | Revised δ (ppm) | |
|---|---|---|---|---|---|
| | | $^1$H | $^{15}$N | $^1$H | $^{15}$N |
| Leu$^{32}$ | A | 8.73 | 130.1 | 8.49 | 128.6 |
| | B | – | – | 8.45 | 128.9 |
| His$^{39}$ | A | 8.77 | 131.0 | 8.79 | 126.9 |
| | B | – | – | 8.65 | 126.5 |
| Asp$^{60}$ | A | 9.01 | 129.8 | 9.05 | 128.8 |
| | B | 8.93 | 130.0 | 8.97 | 129.1 |
| Asp$^{66}$ | A | 8.27 | 122.5 | 8.27 | 129.1 |
| | B | – | – | 8.17 | 128.5 |
| Glu$^{69}$ | A | 8.93 | 128.2 | 8.95 | 130.2 |
| | B | 9.01 | 127.9 | 9.03 | 130.0 |
| Leu$^{79}$ | – | 8.62 | 125.0 | 8.68 | 130.2 |
| Ala$^{88}$ | – | 7.78 | 126.2 | 7.82 | 133.1 |

$^1$H chemical shifts are reported relative to 3-(trimethylsilyl)propionic-$d_4$ acid and $^{15}$N shifts are relative to $^{15}NH_4Cl$ (WGN-01; Wilmad Glass Co.) and reported relative to external liquid $NH_3$. The amino acid sequence is according to Von Bodman et al. (1986) and the sequence numbering is according to Mathews et al. (1979).
[a] Assignments from Guiles et al. (1993).

residues minus 3 prolines). Six pairs of residues showed degenerate intra- and interresidue $C^\alpha$ resonances, which were easily resolved by examination of the HNCOCA spectrum. In all, 10 residues remain unassigned. Possible reasons for lack of correlation peaks corresponding to these unassigned residues are described in the Discussion.

Figure 2 shows 2D slices of the 3D HNCA spectrum, elucidating the sequential connectivity path spanning residues Gly$^{42}$ through Glu$^{56}$. Comparison of Figs. 1 and 2 indicate that differences in the $^{13}C^\alpha$ chemical shift between the A and B forms (e.g., Gly$^{41}$, Val$^{45}$, Leu$^{46}$, etc.) are much smaller than the differences in $^{15}$N chemical shifts for the same residues. For instance, the difference in the $^{15}$N chemical shift between the A and B forms are Gly$^{42}$ (0.3 ppm), Glu$^{43}$ (0.23 ppm), Val$^{45}$ (1.08 ppm) and Leu$^{46}$ (0.4 ppm). In contrast, the $^{13}C^\alpha$ chemical shifts are 0.14, 0.11, 0.24 and 0.00 ppm, respectively, for the same residues. Similar differences are observed for all other residues. Ser$^{71}$ is the only exception, in which case the $^{13}C^\alpha$ chemical shift difference is 1.22 ppm, whereas the $^{15}$N chemical shift difference is 0.23 ppm. Once the backbone $^{13}$C assignments were completed, $H^\alpha$,$H^\beta$ correlations were

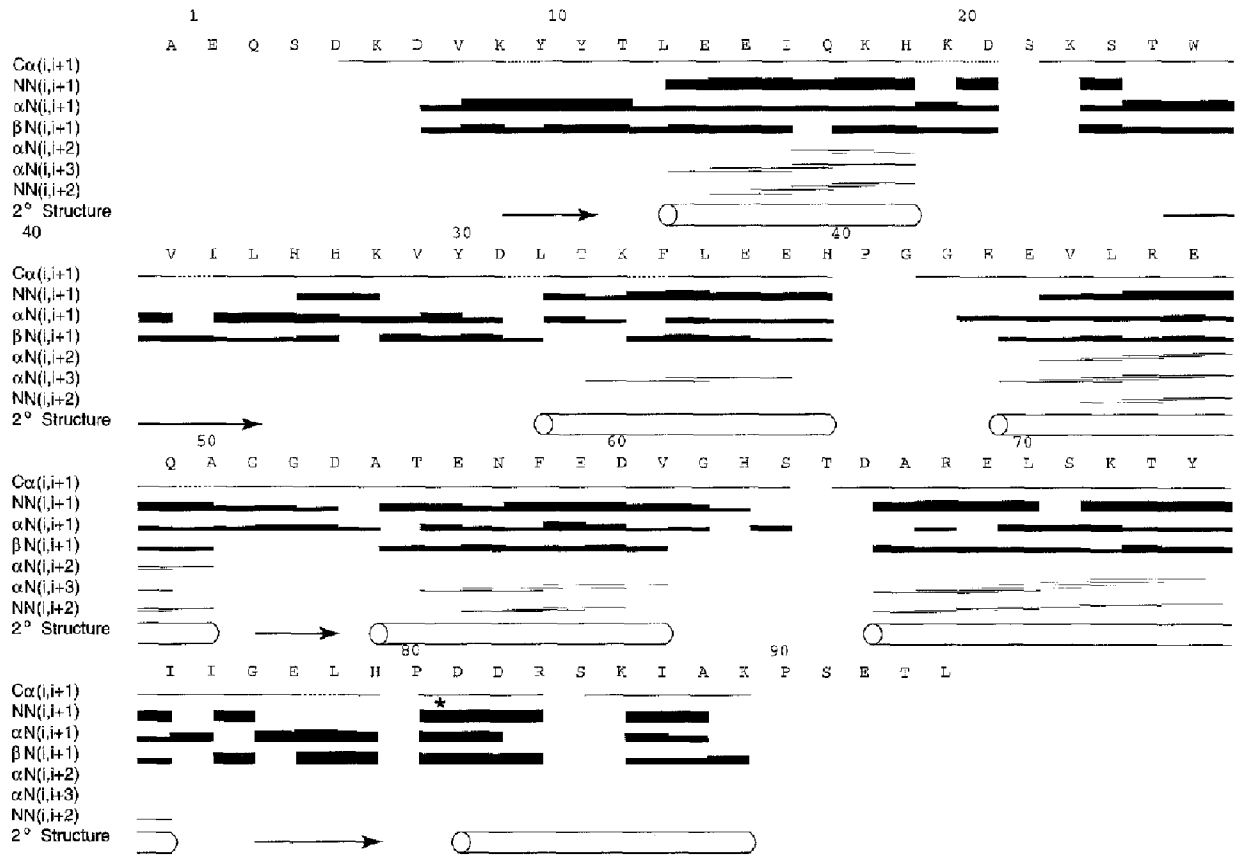


Fig. 4. Assignment diagram summary for rat ferricytochrome $b_5$ based on triple-resonance connectivities and short- and medium-range NOEs involving $H^N$, $C^\alpha H$ and $C^\beta H$ protons. The $C^\alpha$(i,i+1) connectivities shown are those observed in the 3D HNCA experiment. Regions of the protein that contain overlapping intra- and interresidue $C^\alpha$ resonances are indicated by dotted lines. Unassigned residues are indicated by blanks. An asterisk (*) indicates a correlation observed between a δ-proton of proline and $H^N$(i+1). The NOE intensities are indicated by black bars of variable thickness. No correction has been made for the observed intensities due to paramagnetic relaxation. Cylinders depict regions of the backbone that adopt a helical secondary structure, while arrows depict β-sheet elements.

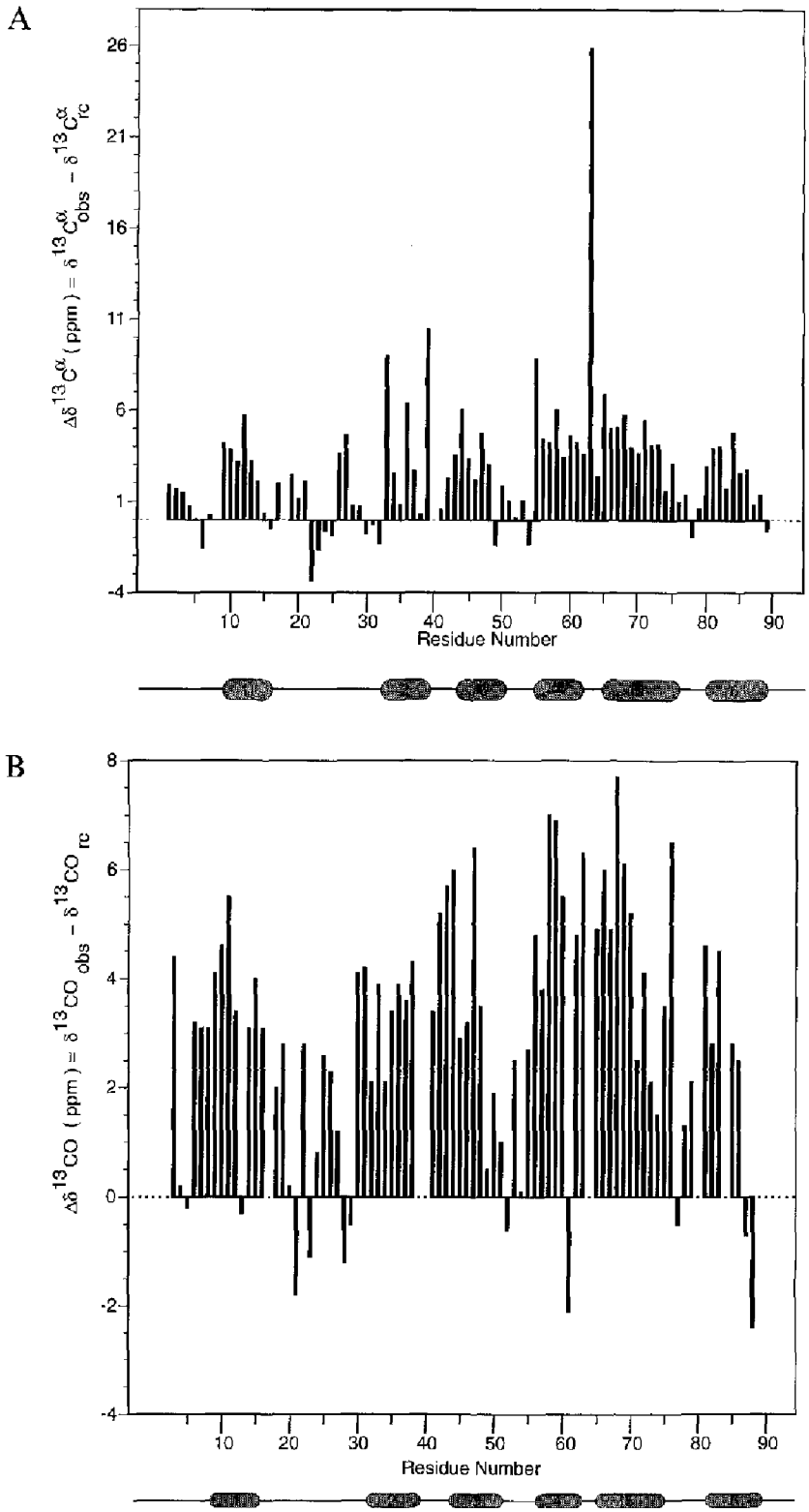


Fig. 5. Secondary $^{13}C$ chemical shifts for rat ferricytochrome $b_5$ are calculated as $\Delta\delta = \delta_{obs} - \delta_{rc}$, where $\delta_{obs}$ are the observed values and $\delta_{rc}$ are the random-coil values (Richarz and Wüthrich, 1978). Panel (A) contains secondary $^{13}C^{\alpha}$ chemical shifts. Unassigned residues are indicated by dotted lines. Helical regions are indicated by cylinders. Due to the similarity in $^{13}C$ chemical shifts of the A and B forms, only the secondary shifts for the A form are shown. Panel (B) contains secondary $^{13}CO$ chemical shifts for rat ferricytochrome $b_5$. Panel (C) contains the predicted contribution to $^{13}C^{\alpha}$ chemical shift from pseudocontact effects, arising from the anisotropic unpaired spin density centered at the metal, as a function of residue number. Predicted shifts are based on pseudocontact shift calculations as described by Emerson and La Mar (1990) and Guiles et al. (1993). As in the case of shifts for protons, carbons closest to the metal center are affected the most. The contribution to the chemical shift is small compared to the chemical shift dispersion of the $^{13}C^{\alpha}$ nucleus in polypeptides. Dotted lines indicate residues that are not observed in the crystal structure. Pseudocontact shifts for these residues are not available.

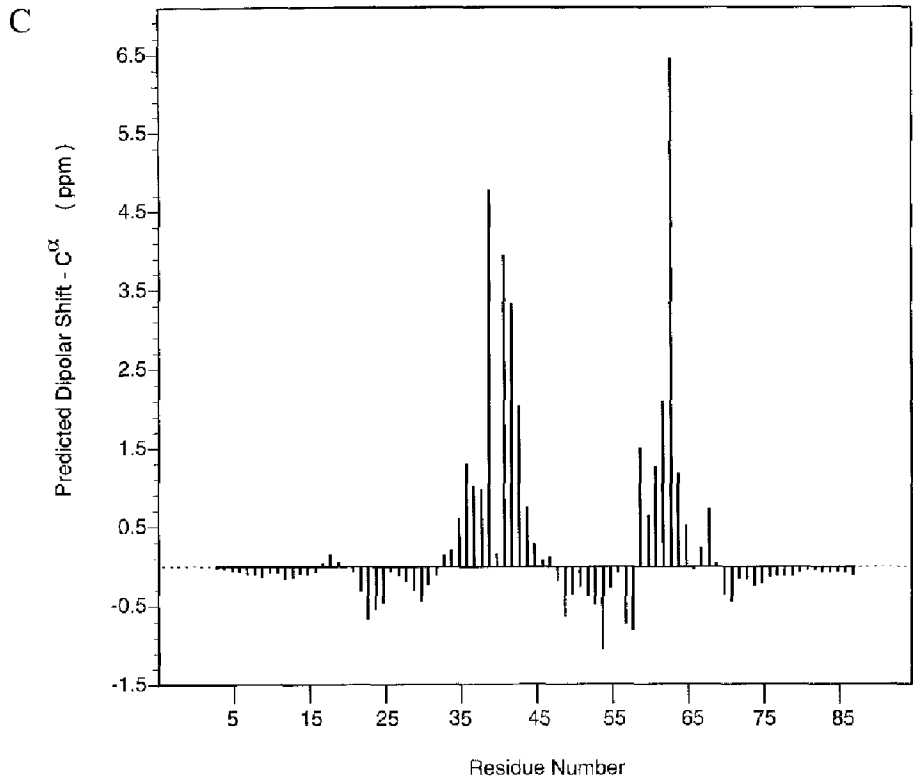


Fig. 5. (continued).

obtained from the $^{15}$N-edited HOHAHA-HMQC spectrum. Sequential resonance assignments were confirmed through identification of short-range $H^NH^N$ (i,i+1), $H^{\alpha}H^N$ (i,i+1), $H^{\beta}H^N$ (i,i+1) correlations in the 3D $^{15}$N-edited NOESY-HSQC spectrum. Identification of medium-range $H^NH^N$ (i,i+2), $H^{\alpha}H^N$ (i,i+2) and $H^{\alpha}H^N$ (i,i+3) connectivities, shown in Fig. 4, provided further confirmation of the sequential assignments. Figure 3 shows the sequential connectivity path observed in the NOESY-HSQC for the same region of the protein as shown in Fig. 2. Once the sequential assignment process was completed, the $C^{\alpha}/H^{\alpha}$, $H^{\beta,\gamma,\delta}$ assignments were used to obtain side-chain carbon-13 assignments using the HCCH-TOCSY spectrum. By this method, side-chain carbon-13 assignments for nearly all residues in the protein were obtained.

On the basis of the above assignment strategy, we propose revised assignments for some of the residues. The reassigned residues are Leu$^{32}$, His$^{39}$, Asp$^{60}$, Asp$^{66}$, Glu$^{69}$, Leu$^{79}$, Ala$^{88}$. The proton and amide nitrogen assignments for these reassigned residues are given in Table 1. With the exception of Leu$^{32}$, the discrepancies in assigned resonances, obtained using the higher resolution and far less ambiguous procedures described herein, are due to the near amide proton coincidences or overlapping clusters of correlation peaks which were not clearly resolved at lower field strengths.

*Secondary structure determination*

The secondary structure determination of rat ferricytochrome $b_5$ was based on the observed NOE correlations among backbone protons and between backbone and side-chain protons. A summary of these NOE correlations from 3D $^{15}$N-edited NOESY-HSQC are presented in Fig. 4. The $^{13}C^{\alpha}$ and $^{13}CO$ chemical shifts presented in Fig. 5, are additional indicators of secondary structure in proteins (Spera and Bax, 1991; Wishart et al., 1991). The nomenclature for the elements of secondary structure is taken from Mathews et al. (1979).

*Helices* Six regions adopting a helical conformation along the polypeptide backbone have been identified on the basis of characteristic short-range $H^NH^N$ (i,i+1), $H^{\alpha}H^N$ (i,i+1), $H^{\beta}H^N$ (i,i+1), and medium-range $H^NH^N$ (i,i+2) and $H^{\alpha}H^N$ (i,i+3) NOE connectivities (Fig. 4). The helical regions are Leu$^9$–His$^{15}$, Leu$^{32}$–His$^{39}$, Glu$^{43}$–Ala$^{50}$, Ala$^{54}$–Val$^{61}$, Asp$^{66}$–Ile$^{75}$ and Asp$^{82}$–Lys$^{89}$. Due to overlap among $H^{\alpha}$ resonances in the helical regions, we have not been able to unambiguously identify many $H^{\alpha}H^N$ (i,i+2) connectivities in the NOESY-HSQC. However, $^{13}C^{\alpha}$ and $^{13}CO$ secondary chemical shifts for residues in these helical regions show down-field shifts from their random-coil values and correspond well to the secondary structure derived by NOEs (Wüthrich, 1986). Although $H^{\alpha}$ chemical shifts are also indicators of secondary structure in proteins, their application to proteins containing an anisotropic paramagnetic center is of limited use because of the 'pseudocontact' (Kurland and McGarvey, 1970) shifts of these resonances caused by the unpaired electron spin.

*β-sheets and turns* There are five segments of extended chain making up the pleated structure in rat cytochrome $b_5$ (Fig. 5): $Lys^5$–$Tyr^7$ ($\beta_1$), $Thr^{21}$–$Leu^{25}$ ($\beta_4$), $His^{27}$–$Tyr^{30}$ ($\beta_3$), $Gly^{51}$–$Asp^{53}$ ($\beta_5$) and $Glu^{78}$–$His^{80}$ ($\beta_2$). Strong $H^{\alpha}H^{N}$ (i,i+1) NOEs as well as up-field-shifted $^{13}C^{\alpha}$ resonances that are characteristic of β-strand secondary structure are observed. Additionally unambiguous long-range NOE connectivities between strands indicate that four chains are parallel and the central chain is antiparallel, forming two parallel and two antiparallel ribbons. We have been able to identify three β-turns in the secondary structure of rat cytochrome $b_5$: $Asp^{17}$–$Ser^{20}$ (I), $Leu^{25}$–$Lys^{28}$ (II), $Gln^{49}$–$Gly^{52}$ (III). On the basis of the observed NOE correlations, Turn II is of type I, while Turn III is of type II. We have been unable to identify the nature of Turn I because of overlap of amide proton resonances of $Asp^{17}$ and $Lys^{19}$ and our inability to identify $Ser^{18}$.

*Unassigned residues*

We believe our inability to assign 10 of 98 residues in the paramagnetic form of rat cytochrome $b_5$ stems from either conformational exchange or solvent exchange at an intermediate time scale or due to enhanced $T_2$ relaxation, due to the presence of the anisotropic paramagnetic center. Absence of correlation peaks assignable to $Pro^{40}$ and only partial sets of correlation peaks associated with $Thr^{65}$ and $Gly^{41}$ are attributable to enhanced relaxation due to the paramagnetic center. Enhanced relaxation due to the paramagnetic center is evident globally through the observation of increases in proton line widths (i.e., most proton line widths are nearly twice those observed for the diamagnetic protein). Anisotropic line-broadening is also evident from a significant variation in peak intensities (for example, in Fig. 1 the $Lys^{34}$, $Asp^{66}$, $Glu^{43}$ and $Glu^{48}$ peaks are discernably weaker than their diamagnetic counterparts). While modified Solomon–Bloembergen equations for anisotropic systems have been proposed (Banci, 1993 and references cited therein), and the paramagnetic anisotropy of this system is well defined (Guiles et al., 1993), at present we have not accurately measured relaxation times nor have we attempted to predict rates based on theory.

The majority of the unassigned residues occur at the N- and C-termini. Of the ten residues that are unassigned, four are at the N-terminus and five residues are at the C-terminus, which are believed to be absent due to conformational or solvent exchange on an intermediate time scale. These regions of the protein are disordered in the crystal structure (Mathews et al., 1979). Presumably missing correlation peaks in these regions are due to enhanced relaxation due to chemical exchange at an intermediate rate. Such effects have been observed in other proteins in flexible loop regions (Stockman et al., 1992). Partial assignments are known for the following residues based on $C^{\alpha}$ to $C^{\alpha}$(i–1) connectivities in the 3D HNCA spectrum; they are: $Asp^1$, $Ser^{18}$, $Gly^{41}$, $Thr^{65}$ and $Ser^{85}$.

## Discussion

Relatively few heme proteins are known for which backbone and side-chain carbon assignments are known through the application of multinuclear, multidimensional NMR, the only other being diamagnetic ferrocytochrome $c_2$ from *Rhodobacter capsulatus* (Caffrey et al., 1994). While the backbone assignments are known for the paramagnetic form of ferricytochrome $c'$ also from *Rhodobacter capsulatus* (Caffrey et al., 1995), our study is the first to provide nearly complete backbone and side-chain assignments for a paramagnetic heme protein. Beside these two heme proteins, only one other paramagnetic protein, *Anabena* 7120 heterocyst ferredoxin (Chae et al., 1993), an iron sulfur protein, has been studied by the use of multidimensional triple-resonance NMR methods. Previous assignments of rat ferricytochrome $b_5$ were accomplished through transfer of assignments from the diamagnetic form to the paramagnetic form (Guiles et al., 1993). This approach employed an iterative procedure involving assignment, followed by a determination of the orientation of the susceptibility tensor, which then allowed prediction of resonances.

Generally, the orientation of the paramagnetic susceptibility tensor is calculated by measuring differences in chemical shifts between redox states and fitting the data to a known structure (usually derived from single crystals by X-ray diffraction) (Emerson et al., 1990; Feng et al., 1990; Veitch et al., 1990). Knowledge of the orientation of the tensor can then enable one to predict shifts of nearly all other atoms. While the method is extremely sensitive, it is prone to errors due to a number of factors: (i) structural differences between the redox states can lead to errors in prediction of magnitude of chemical shifts; (ii) structural differences between the solid and solution states could lead to errors in prediction; and (iii) predictions of shifts of nuclei that lie close to the paramagnetic center (< 7.0 Å) are usually unreliable due to a breakdown of the point-dipole approximation. Most importantly, accurate assignments are essential for prediction of the orientation of the paramagnetic susceptibility tensor. Conventional two-dimensional assignment strategies are complicated by overlap problems caused by broad lines and scrambling of typical connectivity patterns. As can be seen from the above and other studies, three-dimensional heteronuclear double- and triple-resonance NMR offers a rapid method for assigning proteins containing paramagnetic centers (Chae et al., 1994; Caffrey et al., 1995). Unlike ferricytochrome $c'$ and the cyanobacterial ferredoxin, the rat ferricytochrome $b_5$ is low-spin in the oxidized form ($S = 1/2$). This results in longer $T_2$ relaxation times than in cases of proteins with high-spin paramagnetic centers ($S = 5/2$, $S = 2$) (Bertini and Luchinat, 1986) which is the case with both ferricytochrome $c'$ and ferredoxin. As a result we have been able to assign many more residues close to the

paramagnetic center than in earlier studies; 13 and 16 residues for ferredoxin and ferricytochrome *c'*, respectively, all of which lie close to the paramagnetic center, remain however unassigned in these proteins. Data on secondary chemical shifts (Fig. 5) show that, except for residues that serve as ligands ($His^{39}$ and $His^{63}$) for the heme prosthetic group, all residues show the magnitudes of secondary shifts observed in other diamagnetic proteins. Indeed, it was pointed out by Caffrey et al. (1994) that $^{13}C$ chemical shifts are unaffected by ring-current effects, which are also present in paramagnetic heme proteins. Similarly, one would expect that pseudocontact shift effects on $^{13}C$ resonances would also be much less significant, in that, although the magnitude of shift effects are independent of the nucleus, the contribution relative to the intrinsic chemical shift dispersion is small. Consider, for example, the observed shifts for $Gly^{42}$. The geminal proton secondary shifts are 1.94 and 1.63 ppm in the A-form, and 2.08 and 1.74 ppm in the B-form, respectively. Both sets of shifts are substantially different from the random-coil values (Wüthrich, 1986). The $^{13}C^{\alpha}$ secondary shifts of $Gly^{42}$ are 2.3 and 2.4 ppm for the A and B forms, respectively, which are very similar to the values observed in diamagnetic heme proteins (Caffrey et al., 1994). The predicted contribution from pseudocontact shifts for $C^{\alpha}$ resonances of rat cytochrome $b_5$ are shown in Fig. 5C. Secondary chemical shifts arising from secondary structural effects, after corrections for pseudocontact shifts, differ only in magnitude of shifts and not in sign (exceptions being $Gly^{41}$ and $Gly^{42}$). Thus, it appears that $^{13}C$ chemical shifts provide a solid basis for determining the amino acid type, even in paramagnetic proteins where substantial pseudocontact effects are observed. In cases where proton chemical shifts of side-chain atoms are scrambled, $^{13}C$ side-chain assignments would enable us to distinguish between various side-chain atoms. For example, in the assignment of side-chain carbon atoms it was found that the $H^{\gamma'}$ protons of $Ile^{75}$, previously assigned at chemical shifts of 1.21 and 0.76 ppm, are actually 1.22 and –0.23 ppm, respectively. Figure S-3 (Supplementary Material) shows the HCCH-TOCSY spectrum of the $Ile^{75}$ side chain at the $^{13}C$ chemical shift of $C^{\gamma}$. The spectrum arising from a typical AX2 subspin system can be clearly observed, and thus helps in unambiguous assignment of side-chain protons based on the relative insensitivity of the $^{13}C$ chemical shifts to paramagnetic effects. Spin systems of other residue types are also shown in Fig. S-3.

On the whole, the secondary structure of rat ferricytochrome $b_5$ in solution agrees with that obtained from X-ray crystallography. The assignment of helices are in excellent agreement. However, a few small differences are worth noting:

(i) In the crystal structure Helix I extends from $Thr^{8}$–$His^{15}$. The nearly zero $C^{\alpha}$ secondary chemical shift of $Thr^{8}$ suggests that it is not present in a helical domain. In addition, the absence of $H^{\alpha}H^{N}$ (i,i+3) and $H^{N}N^{N}$ (i,i+2) connectivities for residue 8 provides corroborative evidence that $Thr^{8}$ is not part of a helical domain, and hence Helix I is assigned as extending from $Leu^{9}$–$His^{15}$;

(ii) The assignment of Helix III in the crystal structure appears confusing. Two separate reports, one assigning Helix III as $Glu^{43}$–$Gln^{49}$ (Mathews et al., 1979) and the other as $Gly^{42}$–$Gln^{49}$ (Mathews and Czerwinski, 1985). From our data it appears that Helix III extends from $Glu^{43}$–$Ala^{50}$. This is based on the following observations: (a) there are $H^{\alpha}H^{N}$ (i,i+2) and $H^{N}H^{N}$ (i,i+2) connectivities from $Glu^{48}$, and a $H^{\alpha}H^{N}$ (i,i+4) connectivity from $Leu^{46}$; (b) the $Ala^{50}$ $C^{\alpha}$ resonance shows a 2-ppm down-field shift from its random-coil value. Although we do not observe $H^{N}H^{N}$ (i,i+1) between $Gly^{42}$–$Glu^{43}$, the $^{13}C^{\alpha}$ resonances show 2.4-ppm and 3.6-ppm secondary chemical shifts, respectively. As will be discussed below, corrections to observed shifts, from 'pseudocontact' effects show the $C^{\alpha}$ secondary shift of $Gly^{42}$ to be –0.9 ppm and that of $Glu^{43}$ to be 1.6 ppm. This strongly suggests that $Gly^{42}$ is not a part of Helix III. In the case of Helix VI, residues beyond $Ile^{87}$ were not observed in the diffraction data. Once again $^{13}C^{\alpha}$ chemical shifts of $Ala^{88}$ and $Lys^{89}$ seem to indicate that Helix VI could extend out to $Lys^{89}$.

There are some differences in the assignment of β-sheet elements and bends. Several self-consistent pieces of NMR evidence strongly suggest that residues $Ile^{75}$, $Ile^{76}$ and $Gly^{77}$ are not a part of $\beta_2$. No inter-strand $H^{N}H^{N}$ and $H^{\alpha}H^{N}$ connectivities are observed between these residues in $\beta_2$ and residues in $\beta_3$. Also, the $^{13}C^{\alpha}$ chemical shifts do not show characteristic up-field shifts of residues in β-sheets. Additionally, the presence of strong $H^{\alpha}H^{N}$ (i,i+1) between $Ile^{75}$ and $Ile^{76}$, and strong $H^{N}H^{N}$ between $Ile^{76}$ and $Gly^{77}$ suggests that these residues form a part of a turn. It must be mentioned here that in the crystal structure, backbone atoms of residues $Ile^{76}$ and $Gly^{77}$ are thought not to participate in the β-sheet. Based on the above observations we feel justified in not including these residues in the β-sheet. At present, this is a qualitative interpretation of the observed NOE intensities. A structure calculation will reveal further details. We have not been able to confirm the β-bend between $His^{39}$–$Gly^{42}$, because our inability to assign either $Pro^{40}$ or $Gly^{41}$. Residues that are very close to the paramagnetic center are believed to be significantly broadened by dipolar relaxation and are shifted due to pseudocontact effects.

The $His^{39}$ and $His^{63}$ residues ligated to iron show anomalous $^{13}C^{\alpha}$ secondary chemical shifts of 10.47 ppm and 25.92 ppm (5.7 ppm and 19.47 ppm, respectively, after correction for contribution from pseudocontact effects). The difference between the two histidines is even more surprising, given that the backbone torsion angles are nearly identical for both residues (Mathews et al., 1979). Unfortunately, there are no data from other paramagnetic heme systems available for comparison. While the proton-

ation states of these two histidines are well established ($N^{\delta}1$ proton of both histidines are hydrogen-bonded to backbone carbonyl hydrogen-bond acceptors; Mathews et al. 1979), hydrogen bonding alone cannot account for such shifts. In the diamagnetic form of cytochrome $c_2$, Caffrey et al. (1994) have reported a $^{13}C^{\alpha}$ secondary chemical shift of 2 ppm for $His^{17}$ (one of the axial ligands). Large $^{13}C^{\alpha}$ shifts observed in the paramagnetic form of the protein for the axial histidine ligands may be due to inductive effects (Bovey, 1988) of the metal center, or more likely to 'contact' interaction (Walker and Simonis, 1993, and references cited therein) resulting from delocalisation of the unpaired spin. The relative contributions to the observed shifts of $His^{39}$ and $His^{63}$ from either of the effects may be due to differences in side-chain torsion angles between the two residues that are not resolved in the crystal structure.

The relative orientation of the two axial imidazole planes of histidine is thought to modulate heme orbital energy levels, and hence heme reduction potentials (Walker et al., 1986). It is known that the two equilibrium forms of cytochrome $b_5$ possess noncoincident rhombic magnetic axes (Guiles et al., 1993) and the orientation of these appear to track the axial rotation of the heme about its normal (Pochapsky et al., 1990). Based on the observed dipolar shifts, McLachlan et al. (1988) have proposed that the magnetic axes of the heme system in cytochrome $b_5$ are predominantly controlled by axial interaction of heme with $His^{39}$. We have recently prepared site-specific mutants of rat cytochrome $b_5$, designed to perturb the axial ligand-plane orientation of $His^{63}$, and we observed a reorientation of the magnetic axes and a change in reduction potential (Sarma et al., 1996), which suggests that in *bis*-imidazole axially ligated systems, neither imidazole interaction predominates.

Another interesting feature that arises from this study is the similarity of the $^{13}C$ chemical shifts for both isomers, which leads us to the conclusion that the secondary structure of the two forms are virtually identical. As we and others have noted previously (Pochapsky et al., 1990; Guiles et al., 1993), it appears that the heme reorients in its two possible geometries in order to accommodate steric requirements of the rigid hydrophobic binding pocket. As mentioned earlier, differences in $^{13}C^{\alpha}$ chemical shifts for the two forms are much smaller than differences in $^{15}N$ chemical shifts. While it is known that solvation, hydrogen bonding and planarity of the peptide must play key roles in the position of $^{15}N$ chemical shifts, at present we have no detailed explanation for specific differences in $^{15}N$ chemical shifts between isomers. Now that nearly complete assignments for backbone and side-chain atoms are available, it will be possible to calculate solution structures for both equilibrium binding forms of this protein, which will yield insight into the nature of protein–heme recognition factors that control reduction potentials in cytochromes.

Finally, it must be mentioned that the observed differences between crystal and solution structures may only reflect differences in dynamic properties of cytochrome $b_5$ in solution, which could explain some of the missing correlation peaks. A recent molecular dynamics simulation of cytochrome $b_5$ indicates that the molecule is more dynamic in solution than can be inferred from the crystallographic B factors (Storch and Dagget, 1995).

## Conclusions

To our knowledge, in this work the most extensive $^{13}C$ assignments for a highly heterogeneous paramagnetic protein system are presented. The complete $^{13}C$ assignments allow for the correction of errors made in previous $^{1}H$ and $^{15}N$ assignments, and the identification of secondary structural elements in the paramagnetic form of the protein in solution. More importantly, the present work lays the foundation for unambiguous identification of $^{1}H$-$^{1}H$ correlations in $^{13}C$-edited 3D NOESY-HSQC and $^{13}C,^{15}N$ 4D NOESY-HSQC experiments, information which can be used in the calculation of the solution structure of both equilibrium conformers of rat cytochrome $b_5$. Since the orientation of the paramagnetic susceptibility tensor is known for both equilibrium forms of the protein, it can be used as an additional constraint in the refinement of the solution structure (Gochin and Roder, 1995). In addition, extensive assignment of $^{13}C$ will allow for the investigation of backbone and side-chain dynamics by $^{13}C$ relaxation experiments (Nirmala and Wagner, 1988; Palmer III et al., 1991).

## Acknowledgements

We would like to thank Dr. Steven Sligar for the kind gift of the plasmid encoding the soluble heme binding domain of rat cytochrome $b_5$. We would also like to thank Dr. Michael Summers for the use of the NMR spectrometer at the University of Maryland, Baltimore County, and for assistance in the acquisition and processing of spectra. Thanks are also due to Zeneca Pharmaceuticals for allowing the use of their Bruker 500-MHz AMX NMR spectrometer. We also thank the NIH for their generous support of the UMAB NMR Center (1 S10RR10441-01). Thanks also to Dr. Frits Abilgaard for providing triple-resonance gradient sequences for the Bruker Avance system. Financial support from the School of Pharmacy of the University of Maryland at Baltimore is also gratefully acknowledged. Supported by National Institutes of Health Grants DK46510 (R.D.G.).

## References

Banci, L. (1993) In *Biological Magnetic Resonance: NMR of Paramagnetic Molecules*, Vol. 12 (Eds, Berliner, L.J. and Reuben, J.), Plenum Press, New York, NY, pp. 79–111.

Bax, A. and Subramanian, S. (1986) *J. Magn. Reson.*, **67**, 565–570.
Bax, A., Clore, G.M. and Gronenborn, A.M. (1990) *J. Magn. Reson.*, **88**, 425–431.
Bax, A. and Ikura, I. (1991) *J. Biomol. NMR*, **1**, 99–104.
Bax, A. and Pochapsky, S.S. (1992) *J. Magn. Reson.*, **99**, 638–643.
Bax, A. and Grzesiek, S. (1993) *Acc. Chem. Reson.*, **26**, 131–138.
Bertini, I. and Luchinat, C. (1986) In *NMR of Paramagnetic Molecules in Biological Systems* (Eds., Lever, A.B.P. and Gray, H.B.), Benjamin/Cummings Publishing Co., Menlo Park, CA, pp. 47–77.
Bodenhausen, G. and Ruben, D.J. (1980) *Chem. Phys. Lett.*, **69**, 185–188.
Bovey, F.A. (1988) *Nuclear Magnetic Resonance Spectroscopy*, Academic Press, CA.
Caffrey, M., Brutscher, B., Simorre, J.-P., Fitch, J., Cusanovich, M. and Marion, D. (1994) *Eur. J. Biochem.*, **221**, 63–75.
Caffrey, M., Simorre, J.-P., Brutscher, B., Cusanovich, M. and Marion, D. (1995) *Biochemistry*, **34**, 5904–5912.
Chae, Y.K., Abilgaard, F., Mooberry, E. and Markley, J.L. (1994) *Biochemistry*, **33**, 3287–3295.
Cohen, B. and Estabrook, R.W. (1971) *Arch. Biochem. Biophys.*, **143**, 54–65.
Emerson, D.S. and La Mar, G.N. (1990) *Biochemistry*, **29**, 1545–1546.
Feng, Y., Roder, H. and Englander, S.W. (1990) *Biochemistry*, **29**, 3494–3504.
Funk, W.D., Lo, T.P., Mauk, M.R., Brayer, G.D., MacGillivray Ross, T.A. and Mauk, A.G. (1990) *Biochemistry*, **29**, 5500–5508.
Gochin, M. and Roder, H. (1995) *Protein Sci.*, **4**, 296–305.
Grzesiek, S. and Bax, A. (1992) *J. Magn. Reson.*, **96**, 432–440.
Grzesiek, S. and Bax, A. (1993) *J. Biomol. NMR*, **3**, 185–204.
Guiles, R.D., Basus, V.J., Kuntz, I.D. and Waskell, L. (1992) *Biochemistry*, **31**, 11365–11375.
Guiles, R.D., Basus, V.J., Sarma, S., Malpure, S., Fox, K.M., Kuntz, I.D. and Waskell, L. (1993) *Biochemistry*, **32**, 8329–8340.
Hildebrandt, A.G. and Estabrook, R.W. (1971) *Arch. Biochem. Biophys.*, **143**, 66–79.
Hultquist, D.E., Sanes, L.J. and Jackett, D.A. (1984) *Curr. Top. Cell Regul.*, **24**, 287–300.
Imai, Y. and Sato, R. (1977) *Biochem. Biophys. Res. Commun.*, **75**, 420–426.
Kay, L.E., Marion, D. and Bax, A. (1989) *J. Magn. Reson.*, **84**, 72–84.
Kay, L.E., Ikura, M., Tschudin, R. and Bax, A. (1990) *J. Magn. Reson.*, **89**, 496–514.
Keller, R., Groudinsky, O. and Wüthrich, K. (1976) *Biochim. Biophys. Acta*, **427**, 497–511.
Kurland, R.J. and McGarvey, B.R. (1970) *J. Magn. Reson.*, **2**, 286–301.
La Mar, G.N., Burns, P.D., Jackson, J.T., Smith, K.M., Langry, K.C. and Strittmatter, P.J. (1981) *J. Biol. Chem.*, **256**, 6075–6079.
Lee, K.-B., McLachlan, S.J. and La Mar, G.N. (1994) *Biochim. Biophys. Acta*, **1208**, 22–30.
Marion, D. and Wüthrich, K. (1983) *Biochem. Biophys. Res. Commun.*, **113**, 967–974.
Marion, D., Kay, L.E., Sparks, S.W., Torchia, D.A. and Bax, A. (1989a) *J. Am. Chem. Soc.*, **111**, 1515–1517.
Marion, D., Driscoll, P.C., Kay, L.E., Wingfield, P.T., Bax, A., Gronenborn, A.M. and Clore, G.M. (1989b) *Biochemistry*, **29**, 6150–6156.
Marion, D., Ikura, I., Tschudin, R. and Bax, A. (1989c) *J. Magn. Reson.*, **85**, 393–399.
Mathews, F.S., Czerwinski, E.W. and Argos, P. (1979) In *The Porphyrins*, Vol. VIIB (Ed., Dolphin, D.), Academic Press, New York, NY, pp. 107–147.
Mathews, F.S. (1985) *Prog. Biophys. Mol. Biol.*, **45**, 1–56.
McIntosh, L.P., Griffey, R.H., Muchmore, D.C., Nielson, C.P., Redfield, A.G. and Dahlquist, F.W. (1987) *Proc. Natl. Acad. Sci. USA*, **84**, 1244–1248.
McLachlan, S.J., La Mar, G.N., Burns, P.D., Smith, K.M. and Langry, K.C. (1986) *Biochim. Biophys. Acta*, **874**, 274–284.
McLachlan, S.J., La Mar, G.N. and Lee, K.-B. (1988) *Biochim. Biophys. Acta*, **957**, 430–445.
Nirmala, N. and Wagner, G. (1988) *J. Am. Chem. Soc.*, **110**, 7557–7558.
Olejniczak, E. and Eaton, H. (1990) *J. Magn. Reson.*, **87**, 628–632.
Oshino, N. and Sato, R. (1971) *J. Biochem.*, **69**, 169–180.
Palmer III, A.G., Rance, M. and Wright, P.E. (1991) *J. Am. Chem. Soc.*, **113**, 4371–4380.
Pochapsky, T.C., Sligar, S.G., McLachlan, S.J. and La Mar, G.N. (1990) *J. Am. Chem. Soc.*, **112**, 5258–5263.
Richarz, R. and Wüthrich, K. (1978) *Biopolymers*, **17**, 2133–2141.
Rodgers, K.K., Pochapsky, T.C. and Sligar, S.G. (1988) *Science*, **240**, 1657–1659.
Saiki, R.K., Gelfand, D.H., Stoffel, S., Scharf, S.J., Higuchi, R., Horn, G.T., Mullis, K.B. and Erlich, H.A. (1988) *Science*, **239**, 478–494.
Salemme, F.R. (1976) *J. Mol. Biol.*, **102**, 563–568.
Sarma, S., DiGate, R.J., Banville, D. and Guiles, R.D. (1996) manuscript in preparation.
Shimakata, T., Mihara, K. and Sato, R. (1972) *J. Biochem.*, **72**, 1163–1174.
Shinnar, M., Eleff, S., Subramanian, H. and Leigh, J.S. (1989) *Magn. Reson. Med.*, **12**, 74–80.
Sligar, S.G., Egeberg, K.D., Sage, T.J., Morikis, D. and Champion, P.M. (1987) *J. Am. Chem. Soc.*, **109**, 7896–7897.
Spera, S. and Bax, A. (1991) *J. Am. Chem. Soc.*, **113**, 5490–5492.
States, D.J., Haberkorn, R.A. and Ruben, D.J. (1982) *J. Magn. Reson.*, **48**, 286–292.
Stockman, B.J., Nirmala, N.R., Wagner, G., Delcamp, T.J., DeYarman, M.T. and Freisheim, J.H. (1992) *Biochemistry*, **31**, 218–229.
Strittmatter, P. and Velick, S.F. (1956) *J. Biol. Chem.*, **221**, 253–264.
Strittmatter, P., Spatz, L., Corcoran, D., Rogers, M.J., Setlow, B. and Redline, R. (1974) *Proc. Natl. Acad. Sci. USA*, **71**, 4565–4569.
Studier, F.W., Rosenberg, A.H. and Dunn, J.J. (1990) *Methods Enzymol.*, **185**, 113–350.
Veitch, N.C., Whitford, D. and Williams, R.J.P. (1990) *FEBS Lett.*, **269**, 297–304.
Von Bodman, S.B., Schuler, M.A., Jollie, D.R. and Sligar, S.G. (1986) *Proc. Natl. Acad. Sci. USA*, **83**, 9433–9447.
Walker, A.F., Huynh, B.H., Scheidt, R.W. and Osvath, S.R. (1986) *J. Am. Chem. Soc.*, **108**, 5288–5297.
Walker, A.F., Emrick, D., Rivera, J.E., Hanquet, B.J. and Buttlaire, D.H. (1988) *J. Am. Chem. Soc.*, **110**, 6234–6240.
Walker, F.A. and Simonis, U. (1993) In *Biological Magnetic Resonance: NMR of Paramagnetic Molecules*, Vol. 12 (Eds, Berliner, L.J. and Reuben, J.), Plenum Press, New York, NY, pp. 133–148.
Wendoloski, J.J., Mathew, J.B., Weber, P.C. and Salemme, F.R. (1987) *Science*, **238**, 794–797.
Wishart, R., Sykes, B.D. and Richards, F.M. (1991) *J. Mol. Biol.*, **222**, 311–333.
Wüthrich, K. (1986) *NMR of Proteins and Nucleic Acids*, Wiley, New York, NY.
Zuiderweg, E.R.P., Hallenga, K. and Olejniczak, E.T. (1986) *J. Magn. Reson.*, **70**, 336–343.